

1 **Transport and bottom accumulation of fine river**
2 **sediments under typhoon conditions and associated**
3 **submarine landslides: case study of the Peinan River,**
4 **Taiwan**

5
6 **A. A. Osadchiev¹, K. A. Korotenko¹, P. O. Zavialov¹, W.-S. Chiang², and C.-C.**
7 **Liu²**

8 [1]{P.P. Shirshov Oceanology Institute, Moscow, Russia}

9 [2]{Tainan Hydraulics Laboratory, National Cheng-Kung University, Tainan, Taiwan}

10

11 Correspondence to: A. A. Osadchiev (osadchiev@ocean.ru)

12

13 **Abstract**

14 A combination of a three-dimensional Eulerian ocean circulation model (POM) and a
15 Lagrangian particle-tracking model (STRiPE) is used to study the fate of fine river sediments
16 discharged by the Peinan River at the south-eastern coast of the Taiwan Island. The composite
17 model is verified against in situ measurements and applied to simulate primary sediment
18 deposition under freshet and typhoon discharge conditions of the Peinan River. It is shown
19 that local wind plays a crucial role in sediment transport and settling at the coastal area
20 through its influence on the river plume dynamics and turbulent mixing in the upper layer.
21 Wind forcing conditions generally determine the location of the sediment deposit area, while
22 its final pattern is defined by coastal circulation as modulated by the geometry of the coast
23 and local bathymetry. In the study, region river-born sediments are deposited to the sea floor
24 mainly in the shallow shelf areas. A significant portion of discharged fine sediments is moved
25 offshore to the deeper ocean where it is further advected and dispersed by strong coastal
26 circulation mainly governed by the Kuroshio Current.

27 The performed numerical experiments showed that sediment accumulation rate under typhoon
28 conditions is about two orders of magnitude greater comparing to freshet condition. The

1 simulation results were used to identify potential zones of formation of submarine landslides
2 caused by elevated sediment deposition at the steep sea floor during and following the
3 typhoon events. Basing on these results, we identified the areas of the continental shelf and
4 continental slope which exhibit high risk of submarine landslides.

5 **1 Introduction**

6 Small rivers transport significant volume of terrigenous sediment to the ocean in the global
7 scale (Milliman and Syvitski, 1992) and affect short-term and long-term coastal and seabed
8 characteristics (Syvitski and Saito, 2007; Milliman et al., 2007). Particularly, elevated
9 sediment deposit can initiate submarine landslides and subsequent autosuspending turbidity
10 flows, which are frequently observed at certain coastal areas (e.g., Hampton et al., 1996;
11 Lamb and Mohrig, 2009; Carter et al., 2012; Warrick, 2014). One good example are small
12 mountainous rivers of the Taiwan Island delivering 180-380 million tonnes of terrigenous
13 constituents annually. This relatively large discharge is associated with peculiar climatic,
14 topographic, lithological, and anthropogenic features of the Taiwan Island (Dadson et al.,
15 2003; Kao et al., 2005; Kao and Milliman 2008).

16 The major part of riverine water and sediment are discharged from the Taiwan Island during
17 the monsoon season (June-September) when river and sediment runoff are several orders of
18 magnitude greater comparing with the dry season (Warrick and Milliman, 2003; Mirabito et
19 al., 2012). Even more dramatic intensification of the discharge is observed during short-term
20 typhoon events, which were registered 255 times during 1949-2009 (Chang et al., 1993; Liu
21 et al., 2006). On average, 60-80% of sediment load is deposited at the steep eastern and south-
22 western shelves of the island (Liu et al., 2008), which are characterized by elevated seismic
23 activity. Coaction of rapid accumulation and underconsolidation of sediments with earthquake
24 events, which are potential triggers of submarine landslides, has been a subject of
25 considerable research efforts (e.g., Hsu et al., 2008; Huh et al., 2009; Hale et al., 2012; Carter
26 et al., 2012).

27 Energetic turbidity flows can erode and transport huge amount of terrigenous material from
28 shelf areas to the deep sea via submarine canyons (Meiburg and Kneller, 2010; Walsh and
29 Nittrouer, 2009). Taiwan rivers are characterised by high concentrations of total particulate
30 organic carbon (Kao and Liu 1996; Hilton et al. 2008), therefore, turbidity currents at the
31 Taiwan shelf play an important role in burial of organic carbon. Also they have caused a
32 number of destruction events of underwater pipelines, telecommunication cables, and other

1 artificial structures at continental shelf and continental slope (Carter et al., 2014). In
2 particular, a number of cable breaks at the eastern and south-western coastal areas of Taiwan
3 Island happened after a Pingtung Earthquake in 2006, which caused serious failures in data
4 transmission for the whole Asian Pacific region (Hsu et al., 2008). Therefore, identification of
5 coastal areas, which can be potentially influenced by gravity flows, has significant practical
6 importance.

7 Turbidity currents at the Taiwan shelf are mainly caused by two different mechanisms,
8 namely, hyperpycnal river discharge and excrescent accumulation of fine sediment resulting
9 in submarine landslide. The first mechanism which emergences at river estuaries during
10 typhoon events when river sediment concentration exceeds certain value, was considered in
11 many works (e.g., Dadson et al., 2005; Milliman and Kao, 2005; Milliman et al., 2007).
12 However, much less attention was paid to the second mechanism which also can be induced
13 by elevated sediment load during and shortly after typhoon events. It has significantly longer
14 preconditioning period and is characterized by distributed potential sources of turbidity flows
15 (Carter et al., 2014).

16 The present work is focused on the fate of fine sediment discharged by the Peinan River at the
17 north-eastern coast of the Taiwan Island and related identification of areas of potential
18 formation of submarine landslides based on simulated mass distribution of sediment deposit at
19 the seafloor. Previous studies of river-born sediment dispersal in the coastal areas
20 demonstrated its high variability caused by influence of external forcing factors, namely,
21 volume of sediment discharge, sediment concentration in river water, grain-size distribution,
22 coastal flows including tidal circulation, wave forcing and margin geometry (e.g., Orton and
23 Reading, 1993; Walsh and Nittrouer, 2009). Transport of sediments is determined by motion
24 of a buoyant river plume on the one hand and ambient coastal circulation on the other. Many
25 general aspects of sediment delivery to the ocean floor in coastal areas remain unclear
26 (Milliman and Kao, 2005; Yu, 2006). This justifies necessity for research focused specifically
27 on the fate of river-borne sediments, in particular, in the area adjacent to the Peinan River
28 estuary.

29 In this work we use a combination of Lagrangian and Eulerian modelling to reproduce
30 transport and settling of fine terrigenous sediments discharged from the Peinan River. For this
31 purpose, we track these particles as passive tracers of river outflow using a recently developed
32 Lagrangian model called Surface-Trapped River Plume Evolution (STRiPE) applied to the

1 Peinan river plume. After a particle sinks beneath the plume, its movement is governed by
2 coastal circulation simulated by the Princeton Ocean Model (POM). The combination of the
3 models was applied for the study region and validated against in situ measurements. Then we
4 performed numerical experiments to compare the fate of fine sediment under freshet and
5 typhoon forcing conditions and composed respective maps of mass distribution of sediment
6 deposits at the seafloor. Finally, basing on the modelling results and high-resolution
7 bathymetry, we evaluated the probability of formation of typhoon-induced submarine
8 landslides at the study area.

9 The article is organized as follows. Section 2 provides detailed information about the study
10 region and in situ data collected during the field work at the study region in April, 2014 and
11 used for the model validation. Section 3 is focused on the general description and
12 implementation of the joint model. The results of numerical simulations of sediment transport
13 under freshet and typhoon forcing conditions are described in Section 4. Discussion of model
14 results and identification of zones of potential submarine landslides at the study area is given
15 in Section 5, followed by the summary and the conclusions in Section 6.

16

17 **2 Study area**

18 The study region is located at the south-eastern coast of the Taiwan Island, in the area
19 adjacent to the Peinan River estuary (Fig. 1). The oceanographic conditions off the eastern
20 coast of Taiwan are mainly governed by the Kuroshio Current, as well as tides, winds, and
21 river discharge.

22 **2.1 The Kuroshio Current**

23 The Kuroshio Current (KC) originates from the northern branch of the North Equatorial
24 Current (NEC). After bifurcating of NEC near the Philippine archipelago KC passes through
25 the Luzon Strait and flows northward along the eastern coast of the Taiwan Island. On
26 average, KC spans from the eastern coast of Taiwan to 100–150 km offshore and its depth
27 reaches down to 800–1000 m (Liang et al., 2003; Hsin et al., 2008). According to in situ data
28 collected by numerous hydrographic surveys and current meter observations, the northward
29 transport of KC along the eastern coast of Taiwan is estimated to be about 30 Sv (Hsin et al.,
30 2008). However, KC has strong variability ranging from synoptic to inter-annual, in particular
31 at the annual scale it strengthens in summer and weakens in winter (Gilson and Roemmich,

1 2002). However, the position of KC along the coast changes non-uniformly, particularly in
2 winter it moves significantly offshore from the southeastern coast of Taiwan.

3 The mean Kuroshio Central Position (KCP) is located at about 122.1° E southeast of Taiwan
4 and at about 122.9° E northeast of Taiwan, generally following the eastern coastline (Fig. 1).
5 The largest variability of KCP occurs in the area south of 23° N (Hsin et al, 2013), i.e., within
6 the study region of the current work. The climatology of velocity of KC obtained from in situ
7 measurements is rather complex indicating a multicore structure and several branches of KC
8 located to the east of Taiwan (Yuan et al., 1998; Rudnick et al., 2011).

9 As KC sweeps off the southern tip of Taiwan, the main stream passes through the gap
10 between the Taiwan Island and the Green Island (Fig. 2). The speed of KC at this region is
11 about 1.0 m s^{-1} at the top layer (0–200 m), 0.5 m s^{-1} at the middle layer (200 m–400 m), and
12 0.3 m s^{-1} at the bottom layer (400 m–700 m) respectively according to the field measurements
13 (Shen, 2012). The influence of KC is registered till the depth of 800 m, while water below
14 800 m is basically motionless.

15 The small Green Island (about 5 km in diameter) is located at the study region within the
16 energetic mainstream of the KC (Fig. 2). It acts as an obstacle in the stream and induces
17 vortexes shedding downstream from the island, which can be identified at satellite imagery
18 (Liang et al., 2013). A recirculation wake followed by a wavy tail in the lee of the island
19 observed by satellite imagery (Jia and Liu, 2004) and field measurement (Shen, 2012) causes
20 upwelling and enhances nitrate concentration in the upper ocean. This wake covers an area of
21 about 1-2 times greater than the Green Island and is characterized by weak surface current
22 speeds ranging from 0.2 to 0.5 m s^{-1} (Chang et al., 2013).

23

24 **2.2 Tides**

25 In addition to KC, tides play a great role in coastal circulation at the study area. Tidal
26 circulation at this region is mainly governed by four constituents, namely, two semi-diurnal
27 principal solar tides M2 and S2 with periods 12.42 and 12.00 hours respectively, diurnal luni-
28 solar K1, and diurnal lunar O1 with periods 23.93 and 25.82 hours respectively (Wyrtky,
29 1961). A combination of these four components can be used for general description of tidal
30 circulation at the study region.

1 The tidal range is small and tidal currents are weak (Hu et al., 2010; Zu et al., 2008) along the
2 southeastern coast of Taiwan. Tidal sea level harmonic constants (amplitude in cm, phase in
3 degrees) for O1, K1, M2, and S2 were found to be equal to 14.75/79.2, 17.54/101.5,
4 20.6/324.8 and 3.02/67.7 respectively at the tide-gauge station CG (Hu et al., 2010) located in
5 the study region (Fig. 2).

6

7 **2.3 River discharge**

8 Although principal rivers of the Taiwan Island inflow into the Taiwan Strait from the flat
9 western coast, several mountainous rivers of the steeply sloped east coast discharge into the
10 ocean nearly the same amount of suspended sediment (about 150 Mt year⁻¹) as those of the
11 west coast (130-220 Mt year⁻¹) (Liu et al., 2008). The Peinan River is one of the biggest and
12 the most important rivers of the east coast. Despite its modest length (85 km), basin area
13 (1600 km²) and moderate mean annual freshwater runoff varying from 30 m³ s⁻¹ in spring to
14 170 m³ s⁻¹ in summer, the Peinan River discharges a significant volume of sediments equal to
15 20-90 Mt year⁻¹ (Liu et al., 2008; Mirabito et al., 2012). However, river discharge and
16 sediment runoff rates sharply increase during short-term typhoon events frequent in this area.
17 For example, discharge of the Peinan River exceeded 6000 m³ s⁻¹ on 9 August 2009 during
18 typhoon Morakot (Mirabito et al., 2012). The sediment concentration in Peinan water is
19 particularly high following intense precipitation events and can exceed 10 g l⁻¹ (Dadson et al.,
20 2005; Milliman and Kao, 2005).

21

22 **2.4 Bathymetry**

23 Bathymetry of the study region is very complex. For modelling, we chose unfiltered 1/60°
24 resolution (ETOPO1, NOAA) bottom topography. The model domain, as shown in Fig. 2,
25 away the shoreline reveals the wavy deepening relief with two canyons stretched meridionally
26 along 121° E and 121.3° E and separated by an underwater ridge. The model domain includes
27 the Green Island located at 22°50' N and 121°80' E, 40 km off the south-eastern coast of
28 Taiwan. At the eastern flank of the domain the continental slope descends from 1000 m to
29 4000 m.

1 Both canyons merge into the large Taitung Canyon, through which a large volume of
2 sediments derived from the Taiwan mountain belt is transported including heavy sediments
3 and pollutants incoming with the Peinan River waters (Sibuet et al., 2004).

4

5 **3 In situ data**

6 Field survey in the study area was conducted on 15-17 April 2014 using two local fishery
7 boats. Everyday measurements included continuous registration of temperature, salinity, and
8 turbidity in the upper layer along the ship track at the coastal area influenced by the Peinan
9 buoyant plume using a pump-through CTD system equipped with YSI-6600V2 and YSI
10 EXO-2 instruments. In addition, vertical CTD profiling from surface to 25 m depth (or to the
11 seabed at shallower stations) and water sampling were performed at the 14 stations situated as
12 shown at Fig. 3.

13 A portable meteorological station, continuously recording principal meteorological
14 parameters (wind speed and direction, atmospheric pressure, air temperature and humidity) as
15 10 min averages, was mounted about 10 m above the sea level at the top of an old lighthouse
16 2.5 km north of the Peinan River estuary (Fig. 3).

17 The obtained data sets were used for validation of the numerical model reproducing dynamics
18 of the Peinan River plume. The detailed description of model validation and comparison of
19 simulation results with the in situ measurements are given in Section 5.1.

20 The shape, position, and spatial extent of the Peinan river plume showed significant
21 variability during the field survey (Fig. 4, 6). On 15-16 April 2014, the freshwater plume
22 (defined here as the area where salinity was below 33 PSU) was well-developed and stretched
23 along the shore in the southwestern direction from the river mouth. Its alongshore extent and
24 cross-shore width were about 16 km and 3 km, respectively. The inner part of the plume
25 formed a salinity front (25-30 PSU) near the river estuary. On the next day of 17 April 2014,
26 the observed plume was arrested near the estuary and propagated only slightly in the north-
27 eastern direction. The plume area decreased to quarter of its previous size, however, salinity
28 of the inner part of the plume also significantly decreased and was less than 10 PSU. The
29 observed variability of the Peinan river plume was apparently connected with the
30 intensification of wind forcing, which took place on 16 April. The increase of wind stress

1 from less than 0.005 N m^{-2} to about 0.02 N m^{-2} resulted in amplification of plume dispersal
2 and caused development of strong offshore currents and subsequent coastal upwellings.

3

4 **4 Model**

5 As it was mentioned in Section 1, transport of fine sediment discharged from a river has two
6 different phases, one governed by dynamics of buoyant river plume and the other one by
7 ambient coastal circulation. This is the reason for using jointly of two nested numerical
8 models, which complement each other. The outer model is a well-known finite difference σ -
9 coordinate Princeton Ocean Model (POM), which reproduces general ocean circulation along
10 the north-eastern coast of Taiwan with spatial resolution of one minute in latitude and
11 longitude. The outcome from POM provides boundary conditions for the inner Surface-
12 Trapped River Plume Evolution model (STRiPE), which is focused on high-resolution
13 simulation of dynamics of a buoyant river plume. Transport and settling of fine sediment
14 within the nested model is simulated using combination of deterministic approach
15 representing tracking of a passive tracer (James, 2002) and stochastic random-walk scheme
16 parametrizing spatially non-uniform turbulent mixing (Ross and Sharples, 2004). The detailed
17 description of model configuration and its implementation in the present study is given below.

18

19 **4.1 POM module**

20 The POM module consists of a 3D primitive equation ocean model with level 2.5 Mellor–
21 Yamada turbulence closure scheme (Blumberg and Mellor, 1987; Mellor and Yamada, 1982)
22 and complete thermodynamics implemented. The model domain covers the area from 120.9°
23 E to 122.0° E and from 22.3° N to 23.5° N (Fig. 2) and has three open boundaries at the
24 northern, western and southern borders of the region. It is divided into 68×75 grid cells with a
25 size of one minute in both longitudinal and latitudinal directions, i.e., the zonal and
26 meridional resolutions are equal to 1.723 km (at 23° N) and 1.836 km, respectively. The
27 vertical coordinate is represented by 31 σ -levels with irregular vertical spacing. The σ -levels
28 encompass the water column from 5 m to 4860 m stretching in the upper and near-bottom
29 levels for realistic reproducing of surface and bottom boundary layers. The time steps were
30 set equal to 3 s and 120 s for the external and internal modes, respectively.

1 The vertical eddy viscosity and diffusivity were provided by the level 2.5 Mellor–Yamada
 2 turbulence closure scheme with a background value of $10^{-5} \text{ m}^2 \text{ s}^{-1}$. The horizontal eddy
 3 viscosity K_L was calculated using the embedded Smagorinsky formula

$$4 \quad K_L = C_H \Delta x \Delta y \sqrt{\left(\frac{\partial U}{\partial x}\right)^2 + \left(\frac{\partial V}{\partial y}\right)^2 + \frac{1}{2}\left(\frac{\partial U}{\partial y} + \frac{\partial V}{\partial x}\right)^2}, \quad (1)$$

5 where U and V are the horizontal components of the time averaged velocity, C_H is a scaling
 6 parameter equal to 0.1. Horizontal eddy diffusivity was obtained using the inverse Prandtl
 7 number of 0.5.

8 As was mentioned above, the submarine canyons and ridges stretching along the shore are the
 9 important features of the bottom topography. They may significantly affect the structure of
 10 the alongshore flow and mixing governed by the interacting tidal circulation and KC.
 11 Therefore it is important to adequately simulate bottom stress in order to represent these
 12 effects.

13 In the POM module bottom friction is determined by current velocity of the layer closest to
 14 the seabed using the assumption of a logarithmic current profile in the following way. The
 15 stress components τ_b^x and τ_b^y induced by the bottom friction are described as

$$16 \quad \left(\frac{\tau_b^x}{\rho}, \frac{\tau_b^y}{\rho}\right) = C_z (U^2 + V^2)^{1/2} (U, V), \quad (2)$$

17 where C_z is a dimensionless coefficient depending on the roughness length of the bed z_0 and
 18 the water depth H . The coefficient C_z is given by the following formula:

$$19 \quad C_z = \max\left(\frac{\kappa^2}{\{\ln[(1 + \sigma_{kb-1})H / z_0]\}^2}, 0.0025\right), \quad (3)$$

20 where κ is the von Karman constant equal to 0.4, σ_{kb-1} is the depth of the layer overlying the
 21 sea bottom in sigma coordinates.

22 Temperature and salinity boundary conditions applied at the open boundaries of the
 23 calculation domain were different for inflow and outflow fluxes (Fig. 2). Temperature T and
 24 salinity S of inflow water were set equal to the corresponding open boundary values, while in
 25 the case of outflow from the domain the radiation equation was used:

$$26 \quad \frac{\partial}{\partial t}(T, S) + U_n \frac{\partial}{\partial n}(T, S) = 0, \quad (4)$$

1 where n represents the direction normal to the open boundary. The radiation boundary
2 conditions are based on the principle of propagation of a long gravity wave, which is used to
3 specify sea level oscillations in the form of a combination of values of level elevations and a
4 normal current velocity component at the open boundaries.

5 The vertically averaged barotropic velocities at the open boundaries of the model domain
6 were estimated using the Flather (1976) formula:

$$7 \quad \bar{U}_n = \bar{U}_n^0 + \sqrt{\frac{g}{H}}(\eta - \eta_0) \quad (5)$$

8 where \bar{U}_n is the vertically averaged normal component of the time averaged horizontal
9 velocity at the open boundary at the time moment t , \bar{U}_n^0 is the initial vertically averaged
10 normal component, η is the model sea surface elevation calculated using the continuity
11 equation and located half of a grid inside of the open boundary in the model domain, η_0 is the
12 sea surface elevation at the open boundary of the model, H is the water depth on the open
13 boundary, and g is gravitational acceleration. Open boundary conditions \bar{U}_n^0 and η_0 were
14 implemented from the THL barotropic tidal model (Hu et al., 2010) kindly provided by Liu et
15 al. (2014).

16 In this model study we mimicked the Kuroshio Current by specifying an additional surface
17 velocity along the southern boundary of the model domain basing on the observational data
18 and numerical experiments (Yuan et al., 1998; Johns et al., 2001). The additional velocity was
19 determined in the following way. It linearly increased with the distance from the coast, i.e.,
20 from 0 m s^{-1} at the westernmost wet grid point to 0.4 m s^{-1} at the easternmost grid point of the
21 eastern boundary. In vertical dimension we used linearly decreasing velocity from surface to
22 bottom. Since the Kuroshio core is situated beyond the eastern boundary of the model
23 domain, we can apply the simplification described above.

24 **4.2 STRiPE module**

25 STRiPE is a Lagrangian model developed for simulating river plumes under various forcing
26 conditions (Osadchiev and Zavialov, 2013). It represents a river plume as a set of Lagrangian
27 “particles” or homogeneous elementary water columns extending from the surface down to
28 the boundary between the plume and the underlying sea water. These particles are released
29 from the river mouth with the initial velocity depending on the river discharge rate. Then they

1 are tracked by the model according to the momentum equations including the main forces that
2 are applied to individual particles and determine river plume dynamics, namely, the Coriolis
3 force, the wind stress force, the friction with the underlying layer, the lateral friction, the
4 pressure gradient force, and small-scale horizontal turbulent mixing parameterized by the
5 random-walk method. The background velocity field, which is necessary for calculating
6 bottom friction, is imported from POM simulations as input data. At every step of the model
7 integration, the overall set of particles represents the river plume, and hence the temporal
8 evolution of the plume structure is obtained. Horizontal turbulent diffusivity K_h used in the
9 random-walk scheme is parameterized by the Smagorinsky diffusion formula described in
10 Section 3.1. Vertical mixing with the ambient seawater is parametrized by the salinity
11 diffusion equation:

$$12 \quad \frac{\partial S}{\partial t} = K_v \frac{\partial^2 S}{\partial z^2}, \quad (6)$$

13 where S is the salinity, and K_v is the vertical diffusion coefficient parameterized via the
14 Richardson number Ri and scaling coefficient C_v , as given by Large (1994):

$$15 \quad D_v = C_v (1 - \min(1, Ri^2))^3. \quad (7)$$

16 The detailed description of the STRiPE is given in Osadchiev and Zavialov (2013). This
17 model coupled with POM was recently used to study dynamical features of the Zhuoshui and
18 Wu river plumes located at the western part of Taiwan coast (Korotenko et al., 2014).

19

20 **4.3 Sediment transport module**

21 Transport and settling of fine suspended sediments discharged from the river mouth is
22 simulated using a Lagrangian particle-tracking module. Both horizontal and vertical
23 movements of a sediment particle are calculated using a combination of a deterministic
24 component defined by motion of ambient water and sinking of a particle under the gravity
25 force and a stochastic random-walk scheme that reproduces influence of small-scale turbulent
26 mixing. Particles are initially released from the river mouth and their horizontal transport is
27 determined by internal dynamics of a river plume simulated by the STRiPE module. We
28 presume strong mixing in river water before it inflows into the sea, therefore particles have

1 homogenous vertical distribution in the inflowing water. Initial concentration of particles in
2 river water was evaluated according to the following equation (Nash, 1994):

$$3 \quad C = aQ^b \quad (8)$$

4 where C is the sediment concentration in river water, Q is the river discharge volume, a and b
5 are the scaling coefficients.

6 During its motion a particle sinks within the river plume until it reaches the mixing zone
7 between the river plume and the underlying sea waters. After the particle descends beneath
8 the lower boundary of the plume its horizontal motion is determined by ambient coastal
9 circulation calculated by the POM module. In this study we focus on relatively small particles
10 with diameter less than 10^{-4} m, therefore, gravity induced vertical motion is determined by a
11 Stokes' law, and particle settling velocity w_s is calculated according the well-known formula
12 (Stokes, 1851):

$$13 \quad w_s = \frac{gd^2(\rho_s - \rho_w)}{18\mu\rho_w}, \quad (9)$$

14 where g is the gravitational acceleration, d is the diameter of a sediment particle, ρ_s is the
15 density of a sediment particle, ρ_w is the density of water, μ is the dynamic water viscosity.

16 The total vertical displacement of the particle caused by sinking under gravity force, vertical
17 circulation of ambient water, and turbulent mixing was parametrized using the following
18 equation (Hunter et al., 1993; Visser, 1997; Ross and Sharples, 2004), which represents
19 features of spatially non-uniform turbulent mixing:

$$20 \quad \Delta z = \left(w_s + \frac{\partial K}{\partial z} \right) \Delta t + \sqrt{\frac{2}{3} K_v \left(z + \frac{1}{2} \frac{\partial K_v}{\partial z} \Delta t \right)} \Delta t \xi, \quad (10)$$

21 where Δz is the vertical particle displacement, w_s is the Stokes' settling velocity of a particle,
22 K_v is the vertical eddy diffusivity coefficient, Δt is the time step, ξ is a random process with
23 standard normal distribution (zero mean and unity variance) produced by a random number
24 generator.

25 The sediment transport module domain covers the area from 120.9° E to 121.4° E and from
26 22.5° N to 22.9° N and has realistic shoreline. The domain topography was set with a step
27 equal to 0.002° for both latitude and longitude directions with 1 m accuracy.

28

1 5 Numerical simulations

2 The developed model was applied to the study region to investigate the fate of fine sediments
3 discharged by the Peinan River. The POM module was initialized using the Antonov et al.
4 (2010) seasonally averaged climatic temperature and salinity fields as the initial background
5 conditions and provided the ambient velocity fields for the STRiPE and sediment transport
6 modules.

7 In the STRiPE module freshwater particles containing sediment constituents were released
8 from the Peinan River estuary according to the Manning formula with the initial inflow

9 velocity $w = 0.3 \left(\frac{Q}{L} \right)^{2/5}$, where Q is the discharge of the Peinan River, L is the width of the

10 Peinan River mouth. The initial vertical scale of the released freshwater columns (i.e. the

11 plume thickness at the mouth) was prescribed as $h = 3.3 \left(\frac{Q}{L} \right)^{3/5}$. Initial sediment concentration

12 in the inflowing river waters was calculated according to Eq. 8, the coefficients $a = 0.25$ and b
13 $= 0.6$ for $Q < 500 \text{ m}^3 \text{ s}^{-1}$ and $a = 0.02$ and $b = 1.0$ for $Q > 500 \text{ m}^3 \text{ s}^{-1}$ specifying the dependence

14 between river discharge and sediment concentration for the Peinan River under freshet and
15 typhoon conditions were taken from Hwang (1982) and Milliman and Kao (2005),

16 respectively based on gauge measurements performed at the Taitung Bridge (Fig. 3).
17 Densities of river and ambient sea waters were set equal to 1000 kg m^{-3} and 1034 kg m^{-3} ,

18 respectively, while sediment density was prescribed as 2300 kg m^{-3} . The latter value was
19 calculated basing on dry bulk density of sediments delivered by Taiwan rivers to the

20 surrounding seas which was prescribed equal to 1600 kg/m^3 (Liu et al., 2008) and sediment
21 porosity which was set equal to 0.3 (Jiang et al., 2006). Initial grain distribution of fine

22 sediments was prescribed according to the results of analysis of the water samples taken at the
23 1 m depth at the station situated 500 m offshore from the Peinan River mouth (Fig. 3).

24 Kinematic viscosity of water was set equal to $10^{-6} \text{ m}^2 \text{ s}^{-1}$. The integration time steps for the
25 STRiPE and sediment transport modules were set to 10 min.

26 The numerical experiments were organized in the following way. Firstly, we validated the
27 model against the in situ data collected during the field survey. Then we simulated the

28 behaviour of the Peinan river plume and the associated transport of fine sediments under
29 average summer freshet and typhoon conditions.

1 **5.1 Validation**

2 The first simulation was performed under wind forcing and Peinan discharge rate observed
3 during the field work at the meteorological and gauge stations located close to the Peinan
4 estuary (Fig. 3). The period of 15-17 April 2014 was dominated by the south-westerly wind,
5 its speed ranged from 0.5 to 6 m s⁻¹. During this period the Peinan River had constant
6 discharge equal to 21 m³ s⁻¹.

7 The behaviour of the Peinan river plume during 15-17 April 2014 was simulated by the
8 STRiPE module using in situ wind and discharge data and POM-generated current velocity
9 field. The numerical modelling adequately reproduced submesoscale spatial variability of the
10 Peinan River plume observed during the field survey. The Peinan plume was stretched along
11 the shore in south-western direction on 15-16 April, however upwelling-favourable south-
12 western winds resulted in shift of the plume to the north of the Peinan estuary, widening of
13 the plume on 17 April and increase of its salinity anomaly near the estuary. The average
14 positions of the simulated plume corresponding to 16 and 17 April 2014 illustrate this
15 dramatic displacement and show good agreement with the salinity maps of the region
16 obtained from the continuous CTD measurements at the surface layer (Fig. 4).

17 The simulated sediment distribution within the plume was also validated against in situ data.
18 For this purpose we used turbidity measurements performed during the field work at the
19 surface layer and compared them with simulated concentrations of suspended sediments.
20 Turbidity value of 1 NTU was assumed to correspond to suspended concentration value of 0.2
21 g l⁻¹ basing on analysis of water samples taken at station 10. Both field data and numerical
22 modelling showed that surface waters with elevated turbidity corresponded to the position of
23 the plume during the whole simulation period (Fig. 5). Sediment concentration in proximity
24 of the river estuary increased after the shift of the plume on 17 April 2014, which was
25 reproduced by numerical modelling.

26 Vertical haline structure of the Peinan plume and vertical sediment distribution were also
27 consistent with the available in situ data. In particular, dramatic changes of vertical salinity
28 and turbidity profiles measured in proximity of the Peinan river estuary, namely, at stations 8,
29 10, and 12, during 16-17 April were adequately simulated by the numerical model (Fig. 6).
30 Generally, the validation experiment demonstrated good ability of the developed model to
31 reproduce dynamics of the Peinan river plume.

1 **5.2 Numerical experiments**

2 After validation of the model, we performed two numerical experiments simulating the fate of
3 river-born sediments under moderate and flooding discharge conditions of the Peinan River.
4 The first simulation of sediment transport under moderate discharge conditions was executed
5 using average August discharge of the Peinan River ($80 \text{ m}^3 \text{ s}^{-1}$) and average climatic wind
6 conditions (NE wind, 2.0 m s^{-1}). The first experiment was performed for the period of 30
7 days.

8 Model configuration for the second numerical experiment reproducing sediment transport
9 under flooding discharge conditions was more complex. Initially, the plume was modelled
10 under average August climatic conditions for a period of 3 days. After that, we simulated 6
11 days of flooding conditions using wind forcing and discharge rate of the Peinan River
12 observed on 4-9 August 2009, when typhoon Morakot was passing over Taiwan. Next, during
13 the relaxation period the model was forced again by mean climatic conditions for August.
14 Typhoon Morakot induced rainfall over the eastern coast of Taiwan and led to an
15 unprecedented rainfall and subsequent flooding in the southern Taiwan (Wu et al., 2011).
16 Discharge rate of the Peinan River peaked from the annual mean of 80 to $6000 \text{ m}^3 \text{ s}^{-1}$, while a
17 maximal intensity of wind exceeded 40 m s^{-1} (Mirabito et al., 2012).

18 Figure 7f adopted from Mirabito et al. (2012) illustrates discharge rate of the Peinan River
19 before, during, and after typhoon Morakot. Fast and almost uniform increase of discharge of
20 the Peinan River during 7-9 August 2009 was followed by its exponential decrease during 10-
21 16 August 2009. In particular, river discharge sharply dropped during 10 August and then
22 slowly decreased during the following 5 days to the seasonally averaged value. Therefore the
23 decrease rate of the discharge was significantly slower than the increase rate during the whole
24 period except 10 August 2009. The same feature was observed for a number of other Taiwan
25 rivers during the typhoon Morakot (e.g., Gaoping, Zhuoshui, Zengwen, Wu) and was possibly
26 caused by inhomogeneous precipitation distribution during passage of the typhoon Morakot
27 over the Taiwan Island and by relatively small lengths and basin areas of Taiwan rivers
28 (Mirabito et al., 2012).

29 The hydrodynamical model showed a significant impact of typhoon conditions on the sea
30 circulation east of Taiwan and behavior of the Peinan plume. Strengthening of south-westerly
31 winds over the study area and increase of the Peinan River discharge induced by the typhoon
32 resulted in tremendous change of local circulation and considerable elongation of the Peinan

1 plume (Fig 7). Initially, the bulge-like river plume was stretched northwardly along the shore
2 under the action of average climatic winds (Fig. 7a). The interaction of wind drift current and
3 buoyancy resulted in the strong jet-like alongshore current north of the Peinan estuary.

4 The increase of wind stress and change of its direction during the first day of the typhoon
5 caused the plume to widen, to shift in southern direction and to detach from the shore (Fig.
6 7b). During the second typhoon day the plume moved in the northeastern direction, its newly
7 formed part adjacent to the Peinan estuary propagated along the coast, while the older part
8 formed a round-shape bulge, which extension reached the Green Island (Fig. 7c). The third
9 flooding day was characterized by peaks of wind speed, river discharge, and velocity of
10 coastal circulation (1 m s^{-1}). For this day, the plume was stretched north-eastwardly and
11 detached from the coast near 23° N (Fig. 7d). Figure 7e shows the Peinan plume on 10 August
12 2009 when discharge rate decreased below $2000 \text{ m}^3 \text{ s}^{-1}$, but wind remained strong with its
13 speed exceeding 10 m s^{-1} . During this period the meandering plume became unstable in its
14 near-field and was broken into several patches. The far-field of the plume remained
15 consolidated, but its salinity contrasts with the ambient water noticeably diminished. After the
16 departure of the typhoon from the study area, the north-eastward current was decreasing
17 gradually during several next days. The Peinan plume was tending to return to its position and
18 shape as they were before the typhoon (Fig. 7a).

19 The simulated spread of the Peinan river discharge in coastal waters during typhoon Morakot
20 showed similar characteristics with the discharges of other large Taiwan rivers. As described
21 in (Chien et al., 2011; Jan et al., 2013) major rivers of the western Taiwan, namely, the
22 Zhuoshui, Wu, Tsengwen, and Gaoping rivers, formed large buoyant plumes. Together with
23 surface-advected plumes, these rivers (characterized by elevated suspended sediment
24 concentration) also produced hyperpycnal flows (Milliman and Kao, 2005; Carter et al.,
25 2012), which, however, lay beyond the scope of our current research. Horizontal ($\sim 100 \text{ km}$)
26 and vertical ($\sim 10 \text{ m}$) spatial scales as well as salinity anomaly ($\sim 2 \text{ PSU}$) of the far-field part of
27 the buoyant plume formed by the Zhuoshui River based on in situ measurements performed
28 on 13-17 August 2009 are the same as those simulated by the numerical model for the Peinan
29 plume shortly after the typhoon Morakot (Fig. 7e) (Jan et al., 2013). Lifetimes of these large
30 freshwater plumes were also similar, they returned to their pre-typhoon states about 1-1.5
31 weeks after river discharges dropped to their average monthly values (Jan et al., 2013).

32

1 **6 Results and discussion**

2 **6.1 Sediment deposition**

3 The obtained simulation results of river-born sediment delivery after 30 days of freshet
4 conditions and 6 days of the typhoon are presented at Fig. 8. Sediment outflow concentration
5 in the Peinan River water was about 4 kg m^{-3} during the moderate discharge simulation,
6 which result in $0.8 \cdot 10^6$ tons of sediment discharge for the period of 30 days. Typhoon
7 conditions were characterized by dramatic increase of river runoff and sediment concentration
8 with the peak values of about $6000 \text{ m}^3 \text{ s}^{-1}$ and 120 kg m^{-3} correspondingly. The total sediment
9 influx during the 6 typhoon days was about $20 \cdot 10^6$ tons, which is 25 times greater comparing
10 to the moderate discharge simulation for 30 consecutive days. As a result, the sediment
11 accumulation rate under typhoon discharge conditions was about two orders of magnitude
12 greater comparing to average freshet discharge.

13 The resulting deposit patterns obtained by the two model runs were significantly different.
14 During freshet discharge period river-born sediments were almost homogenously deposited at
15 the shallow area in the southern and south-western directions from the river estuary. The
16 alongshore extent of the area influenced by active sediment load ($3\text{-}5 \text{ kg m}^{-2}$) exceeded 25
17 km. Total sediment load to the seabed at the study area was about $0.5 \cdot 10^6$ tons, while $0.3 \cdot 10^6$
18 tons of fine sediments remained in water column and did not settle to the sea floor during the
19 simulation period.

20 The most active sediment load during and shortly after typhoon period took place within the
21 small area adjacent to the Peinan River estuary. The spatial scale of this area was only 5 km,
22 however, the mass of sediment that settled to the bottom exceeded 300 kg m^{-2} . A large
23 volume of sediment was also transported form the Peinan River mouth along the shore in the
24 south-western and north-eastern directions and settled to the seabed at the corresponding
25 shallow shelf areas. The spatial extents and bottom sediment concentrations at the considered
26 coastal zones influenced by active sediment loads were equal to 10 km and $150\text{-}250 \text{ kg m}^{-2}$ for
27 the south-western zone and 5 km and $50\text{-}150 \text{ kg m}^{-2}$ for the north-eastern zone. However, only
28 about $8 \cdot 10^6$ tons of the total sediment discharge volume settled at the sea floor within the
29 study area, while $12 \cdot 10^6$ tons were transported offshore to the deeper sea and remained in the
30 water column.

1 The presented simulation results show that sediment deposition patterns for both model runs
2 significantly depend on the river plume dynamics. Under freshet discharge conditions and
3 moderate wind forcing the alongshore transport of the Peinan plume is generally in
4 geostrophic balance. As a result, river-born sediments which are initially concentrated in the
5 upper layer, are transported by the plume in the south-western direction. Once sediment
6 particles sink beneath the plume, their motion is determined by the north-eastward coastal
7 circulation governed by the KC. The average velocity of coastal currents below the upper
8 layer is significantly smaller than the velocity of the river plume propagation. Therefore,
9 sediment particles settled from the plume to the underlying waters at shallow coastal areas
10 located to the south-western from the Peinan estuary are only slightly displaced by coastal
11 currents in the north-eastern direction and are finally deposited to the seabed at this area. On
12 the other hand, a significant portion of sediments at the study region is transported by the
13 plume offshore from the narrow continental shelf. Once these sediment particles sink beneath
14 the plume at deeper ocean, they are moved away in the north-eastward direction by the strong
15 alongshore current and do not settle at the sea floor within the study region.

16 Elevated discharge of terrigenous sediments to the sea during typhoon conditions resulted in
17 increased sediment deposit at the study area. However, the rate of deposited sediments in
18 respect to the total discharge (40%) was significantly lower comparing to the freshet
19 conditions (65%) because of the following reasons. Typhoon conditions are characterized by
20 strong winds, which governed the spread of the Peinan plume at the study region. During the
21 simulation period the Peinan plume propagated mostly in the north-eastern direction,
22 therefore the river-borne sediments settled mainly in the small shallow area immediately
23 adjacent to the river plume. Also, the plume propagation velocity was significantly higher
24 comparing to the freshet conditions, therefore, the major part of the sediments did not sink
25 beneath the plume within this shallow area and were transported offshore to the deeper ocean.
26 Finally, strong wind forcing induced active turbulence at the upper layer, which reduced
27 settling speed of the sediment particles. A short period of northern winds during the typhoon
28 resulted in active sediment deposition at the shallow coastal area situated to the south from
29 the Peinan estuary, however, the volume of sediment load at this area was much less
30 comparing to the area adjacent to the Peinan estuary. The obtained simulation results are
31 consistent with the findings of the previous studies (Milliman and Kao, 2005; Kao et al.,
32 2008) that the ratio of fine sediments deposited at coastal waters to the total sediment

1 discharge is significantly lower during typhoon events comparing with average climatic
2 conditions.

3 **6.2 Submarine landslides**

4 One of the practical aims of this study consists in identification of the zones at the study area
5 which exhibit elevated risk of formation of submarine landslides caused by elevated sediment
6 deposit after typhoon events. Such landslides can cause autosuspending gravity flows at the
7 steep continental slope. For instance, two cable-breaking gravity flows were registered after
8 the typhoon Morakot near the Gaoping River estuary in the south-western part of the Taiwan
9 Island (Carter et al., 2012; Su et al., 2014). The first one happened on 9 August 2006 and was
10 caused by a hyperpycnal flow of the Gaoping discharge, while the second one took place on
11 13 August 2006 and was associated with submarine landslide of rapidly deposited sediment
12 during and shortly after the typhoon event.

13 However, in this study we focus on dependences of sediment deposit patterns on external
14 forcing conditions as one of the major preconditioning factor of formation of a submarine
15 landslide. Using the simulated distribution of the mass of sediment deposit we can calculate
16 the downslope component of gravity force applied to the sediment in the following way: $F =$
17 $m \cdot g \cdot \sin(\alpha)$, where m is the mass of sediment deposit to the considered unit seabed area and α
18 is the local bottom slope angle. This value is proportional to the rate of overpressure, which
19 cause a submarine landslide if exceeds a certain value, which depends on local bottom
20 friction. Thus, seabed areas with high values of F are the potential regions of formation of
21 autosuspending gravity flows.

22 We considered the distribution of F for typhoon conditions because for this case the average
23 “sliding” force was several orders greater than that for sediment distributions formed under
24 moderate discharge conditions. Figure 9 illustrates three characteristics which are related to
25 formation of submarine landslides and gravity flows, namely, bottom topography gradient
26 (Fig. 9a), distribution of F normalized by its maximal value in the study region (Fig. 9b), and
27 paths of the turbidity flows potentially caused by submarine landslides within the study region
28 (Fig. 9c). Every point of the seafloor where a submarine landslide can be potentially
29 generated “produces” a single path which is assumed to propagate in direction of maximal
30 topography gradient. Saturation of color of a path corresponds to the saturation of color of its
31 initial point, i.e., dark/light red paths illustrate more/less likely gravity flows. If two different

1 paths (with different saturations of their colors) go through the same point, the more plausible
2 path is drawn.

3 As it can be seen from the figures, the most risky region with respect to formation of
4 submarine landslides at the study area is located near the Peinan River estuary, which is
5 characterized by the most active sedimentation under typhoon conditions. Pathways of the
6 turbidity flows generated in this zone cover large coastal area situated to the south-east from
7 the Peinan River estuary. This area is significantly different from the potential path of the
8 gravity flow caused by hyperpycnal Peinan plume.

9 Two gravity flows of different origin registered near the Gaoping River estuary after the
10 typhoon Morakot also had different formation points and different paths according to the
11 locations of the underwater cable breaks. The first turbidity current was formed by a
12 hyperpycnal flow in proximity of the river estuary, while the second one (presumably caused
13 by a submarine landslide) originated about 10 km far from the estuary about 3 days after the
14 peak discharge (Carter et al., 2012). These spatial and temporal scales are similar to our
15 findings concerning the Peinan River.

16

17 **7 Summary and conclusions**

18 This study is focused on influence of external forcing conditions on transport and deposition
19 of fine sediment discharged from the Peinan River at the steep north-eastern coast of the
20 Taiwan Island. For this purpose, we used a combination of two hydrodynamic numerical
21 models, namely, the Eulerian Princeton Ocean Model (POM) and the Lagrangian Surface-
22 Trapped River Plume Evolution (STRiPE) model. The combined model was validated against
23 in situ measurements performed in the study area on 15-17 April 2014. Then it was used to
24 simulate the fate of river-borne sediments discharged during a typical freshet period and
25 during a strong typhoon. For the first numerical experiment we used average climatic August
26 discharge and wind forcing conditions, while the second model run was performed under real
27 forcing conditions observed during the Morakot typhoon on 4-9 August 2009.

28 Numerical experiments showed that the initial transport of terrigenous material is mainly
29 governed by river plume dynamics, while its final deposition depends on the ambient coastal
30 circulation as modulated by the local bathymetry. In particular, the most active sediment
31 deposition at the study region took place in the shallow shelf areas. Sediment particles which

1 were initially transported by the river plume offshore to the continental slope and deep sea
2 were advected and dispersed by strong coastal circulation governed by the Kuroshio Current
3 before they reached the sea floor.

4 Strong wind forcing during the typhoon wind increased turbulence in the upper layer and,
5 therefore, decreased sediment settling speed during its transport by the river plume. On the
6 other hand, elevated wind stress resulted in high velocity of plume propagation. 5 In
7 consequence, a larger fraction of sediments was transported offshore from the shallow shelf
8 before it sank beneath the plume. These factors resulted in a lower ratio of sediment deposit
9 volume to total sediment influx comparing to freshet conditions.

10 Elevated sediment runoff during typhoon event can result in submarine mudslides at the areas
11 of active sediment loads. Basing on the simulation results, we identified zones within the
12 study area characterized by high possibility of submarine landslide formation. In addition, we
13 identified the potential pathways of autosuspending gravity flows induced by the submarine
14 landslides. The obtained results may have practical implications related to construction of
15 artificial structures such as telecommunication cables and underwater pipelines on the
16 seafloor in the study region.

17

18 **Acknowledgements**

19 Funding of this research was provided by Russian Scientific Foundation, research project 14-
20 50-00095 (model development and numerical experiments) and Tainan Hydraulics
21 Laboratory, National Cheng-Kung University, Taiwan (field work and data analyses).
22 Authors wish to thank Aleksandr Izhitsky and Aleksandr Grabovsky for valuable support
23 during the fieldwork, Marina Kravchishina for granulometric analysis of water samples, and
24 many colleagues at THL for their hospitality and assistance. This article benefited from
25 critical comments and constructive suggestions from two anonymous reviewers.

26

1 **References**

- 2 Antonov, J. I., Seidov, D., Boyer, T. P., Locarnini, R. A., Mishonov, A. V., Garcia, H. E.,
3 Baranova, O. K., Zweng, M. M., and Johnson, D. R.: World Ocean Atlas 2009, Volume 2:
4 Salinity, edited by: Levitus, S., NOAA Atlas NESDIS 69, U.S. Gov. Printing Office,
5 Washington, D.C., 184 pp., 2010.
- 6 Blumberg, A.F. and Mellor, G.L., 1987. A description of a three-dimensional hydrodynamic
7 model of New York harbor region. *Journal of Hydraulic Engineering*, 125, 799–816.
- 8 Carter, L., J.D. Milliman, P.J. Talling, R. Gavey, and R.B. Wynn, 2012. Near-synchronous
9 and delayed initiation of long run-out submarine sediment flows from a record-breaking river
10 flood, offshore Taiwan. *Geophysical Research Letters*, 39, L12603.
- 11 Carter, L., R. Gavey, P. Talling, and J. Liu, 2014. Insights into submarine geohazards from
12 breaks in subsea telecommunication cables. *Oceanography*, 27, 58-67.
- 13 Chao, S.Y., 1988. River-forced estuarine plume. *Journal of Physical Oceanography* 18, 72–
14 88.
- 15 Chang, C-P., Yeh, T-C., and Chen, J.M., 1993. Effects of Terrain on the Surface Structure of
16 Typhoons over Taiwan. *Monthly Weather Review*, 121, 734–752.
- 17 Chang, M.-H., T. Y. Tang, C.-R. Ho, and S.-Y. Chao, 2013. Kuroshio-induced wake in the lee
18 of Green Island off Taiwan. *Journal of Geophysical Research: Oceans*, 118, 1508–1519.
- 19 Chien, H., W.-S. Chiang, S.-J. Kao, J.T. Liu, K.-K. Liu, and P.L.-F. Liu, 2011. Sediment
20 dynamics observed in the Jhoushuei River and adjacent coastal zone in Taiwan Strait.
21 *Oceanography*, 24, 123-131.
- 22 Chuang, W.-S., 1985. Dynamics of subtidal flow in Taiwan Strait. *Journal of Oceanographic*
23 *Society of Japan*, 41, 65–72.
- 24 Chuang, W.-S., 1986. A note on the driving mechanisms of current in Taiwan Strait. *Journal*
25 *of Oceanographic Society of Japan*, 42, 355–361.
- 26 Dadson, S., Hovius, N., Pegg, S., Dade, W.B., Horng, M.J., and Chen, H., 2005. Hyperpycnal
27 river flows from an active mountain belt. 11, F04016.
- 28 Flather, R.A., 1976. A Tidal Model of the North-West European Continental Shelf. *Memoires*
29 *de la Societe royale des sciences de Liege*, 10, 141–164.

- 1 Fong, D.A., Geyer, W.R., 2002. The alongshore transport of freshwater in a surface trapped
2 river plume. *Journal of Physical Oceanography* 32, 957–972.
- 3 Garcia Berdeal, I., Hickey, B.M., Kawase, M., 2002. Influence of wind stress and ambient
4 flow on a high discharge river plume. *Journal of Geophysical Research*, 107, 3130–3151.
- 5 Garvine, R.W, 1987. Estuary plumes and fronts in shelf waters: a layer model. *Journal of*
6 *Physical Oceanography* 17, 1877–1896.
- 7 Geyer, W.R., Hill, P.S., Kineke, G.C., 2004. The transport, transformation and dispersal of
8 sediment by buoyant coastal flows. *Continental Shelf Research*, 24, 927-949.
- 9 Gilson, J., and D. Roemmich, 2002. Mean and temporal variability of Kuroshio geostrophic
10 transport south of Taiwan (1993–2001). *Journal of Oceanography*, 58, 183–195.
- 11 Hale, R.P., C.A. Nittrouer, J.T. Liu, R.G. Keil, and A.S. Ogston, 2012. Effects of a major
12 typhoon on sediment accumulation in Fangliao Submarine Canyon, SW Taiwan. *Marine*
13 *Geology*, 326, 116-130.
- 14 Hampton, M.A., H.J. Lee, and J. Locat, 1996. Submarine landslides. *Reviews of Geophysics*,
15 34, 33-59.
- 16 Hilton, R.G., A. Galy, and N. Hovius, 2008. Riverine particulate organic carbon from an
17 active mountain belt: importance of landslides. *Global Biogeochemical Cycles*, 22, GB1017.
- 18 Hsin, Y.-C., B. Qiu, T.-L. Chiang, and C.-R. Wu, 2013. Seasonal to interannual variations in
19 the intensity and central position of the surface Kuroshio east of Taiwan. *Journal of*
20 *Geophysical Research*, 118.
- 21 Hsin, Y.-C., C.-R. Wu, and P.-T. Shaw (2008), Spatial and temporal variations of the
22 Kuroshio east of Taiwan, 1982–2005: A numerical study. *Journal of Geophysical Research*,
23 113, C04002.
- 24 Hsu, S.-K., Kuo, J., Lo, C.-L., Tsai, C.-H., Doo, W.-B., Ku, C.-Y., and Sibuet, J.-C., 2008.
25 Turbidity Currents, Submarine Landslides and the 2006 Pingtung Earthquake off SW Taiwan.
26 *Terrestrial, Atmospheric and Ocean Sciences*, 19, 767-772.
- 27 Hu, C.K., Chiu, C.T., Chen, S.H., Kuo, J.Y., Jan, S., and Tseng, Y.H., 2010. Numerical
28 simulation of barotropic tides around Taiwan. *Terrestrial Atmospheric and Oceanic Sciences*,
29 21, 71–84.

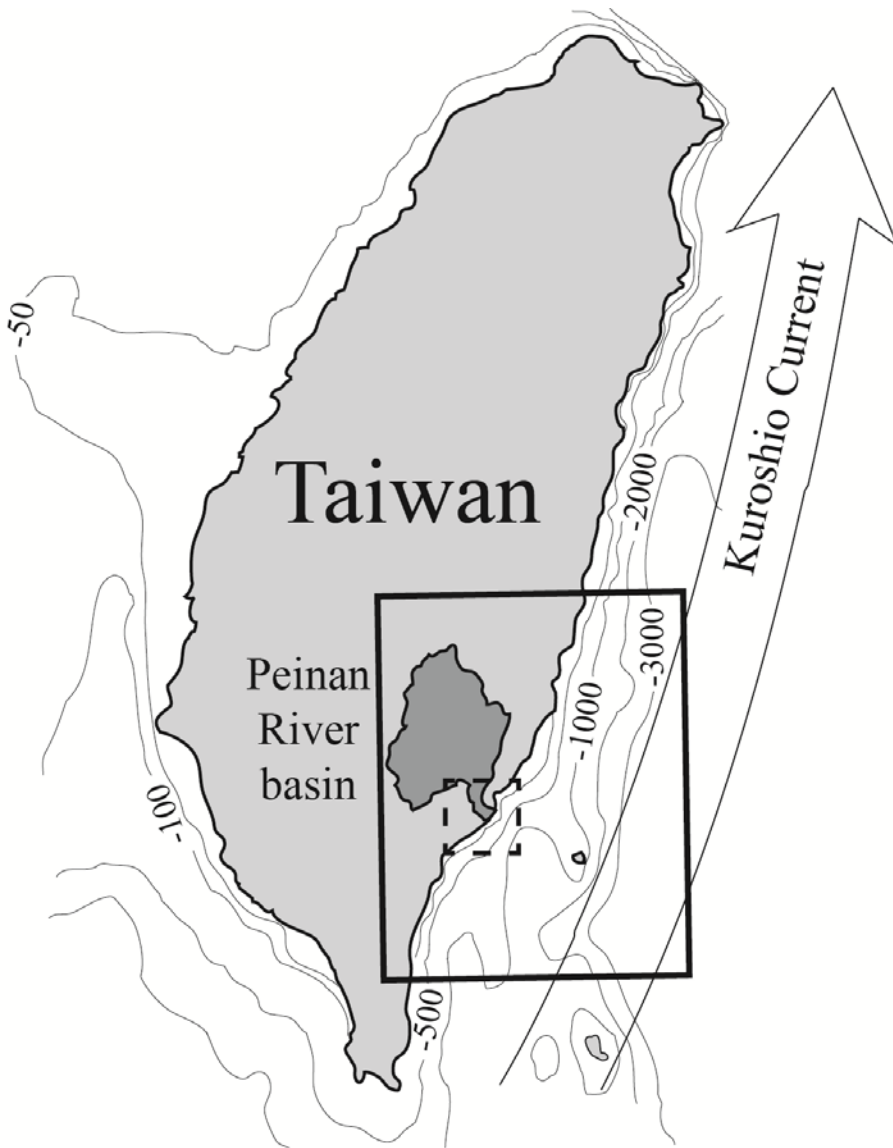
- 1 Huh, C.-A., H.-L. Lin, S. Lin, and Y.-W. Huang, 2009. Modern accumulation rates and a
2 budget of sediment off the Gaoping (Kaoping) River, SW Taiwan: A tidal and flood
3 dominated depositional environment around a submarine canyon, *Journal of Marine Systems*,
4 76, 405–416.
- 5 Hunter, J.R., 1987. Application of Lagrangian particle-tracking technique to modeling of
6 dispersion in the sea. In: Noye, J. (Ed.), *Numerical Modelling: Applications for Marine*
7 *Systems*. North Holland, Amsterdam, 257–269.
- 8 Hunter, J.R., Craig, P.D., and Phillips, H.E., 1993. On the use of random walk models with
9 spatially variable diffusivity. *Journal of Computational Physics*, 106, 366-376.
- 10 Hwang, C., 1982. Suspended sediments of Taiwan rivers and their geomorphological
11 significance. *Bulletin of Nation Taiwan Normal University*, 27, 649-677.
- 12 James, I.D., 2002. Modelling pollution dispersion, the ecosystem and water quality in coastal
13 waters: a review. *Environmental Modelling and Software*, 17, 363-385.
- 14 Jan, S., Chern, C.-S., and Wang, J., 2002. Transition of tidal waves from the East to South
15 China Sea over Taiwan Strait: influence of the abrupt step in the topography. *Journal of*
16 *Oceanography*, 58, 837–850.
- 17 Jan, S., Wang, J., Yang, Y. J., Hung, C. C., Chern, C. S., Gawarkiewicz, G., Lien, R.-C.,
18 Centurioni, L., Kuo, J.-U., and Wang, B.: Observations of a freshwater pulse induced by
19 Typhoon Morakot off the northern coast of Taiwan in August 2009. *Journal of Marine*
20 *Research*, 71, 19-46, 2013.
- 21 Jia, Y. and Liu, Q., 2004. Eddy shedding from the Kuroshio bend at Luzon Strait. *Journal of*
22 *Oceanography*, 60, 1063–1069.
- 23 Jiang, W.-T., Chen, J.-C., Huang, B.-J., Chen, C.-J., Lee, Y.-T., Huang, P.-R., Lung, C.-C.,
24 and Huang, S.-W., 2006. Mineralogy and physical properties of cored sediments from the gas
25 hydrate potential area of offshore southwestern Taiwan. *Terrestrial Atmospheric and Oceanic*
26 *Sciences*, 17, 981-1007.
- 27 Johns, W.E., Lee, T.N., Zhang, D., Zantopp, R., Liu, C.-T., and Yang, Y., 2001. The
28 Kuroshio East of Taiwan: Moored Transport Observations from the WOCE PCM-1 Array.
29 *Journal of Physical Oceanography*, 31, 1031-1053.

- 1 Kao S.-J., and K.-K. Liu, 1996. Particulate organic carbon export from a subtropical
2 mountainous river (Lanyang-His) in Taiwan. *Limnology and Oceanography*, 41, 1749-1757.
- 3 Kao, S.-J., Chan, S.C., Kuo, C.H., Liu, K.K., 2005. Transport-dominated sediment loading in
4 Taiwanese rivers: a case study from the Ma-an Stream. *Journal of Geology*, 113, 217–225.
- 5 Kao, S.- J., Jan, S., Hsu, S.-C., Lee, T.-Y., and Dai, M., 2008. Sediment budget in the Taiwan
6 Strait with high fluvial sediment inputs from mountainous rivers: New observations and
7 synthesis. *Terrestrial, Atmospheric and Oceanic Sciences*, 19, 525-546.
- 8 Kilcher, L.F., Nash, J.D., and Moum, J.N., 2012. The role of turbulence stress divergence in
9 decelerating a river plume. *Journal of Geophysical Research*, 117, C05032.
- 10 Korotenko, K.A., A.A. Osadchiv, P.O. Zavialov, R.-C. Kao, and C.-F. Ding, 2014. Effects of
11 bottom topography on dynamics of river discharges in tidal regions: case study of twin
12 plumes in Taiwan Strait. *Ocean Science*, 10, 865-879.
- 13 Lamb, M.P. and D. Mohrig, 2009. Do hyperpycnal-flow deposits record river-flood
14 dynamics? *Geology*, 37, 1067-1070.
- 15 Large, W.G., McWilliams, J.C., Doney, S.C., 1994. Oceanic vertical mixing: a review and a
16 model with a nonlocal boundary layer parameterization. *Reviews of Geophysics* 32, 363–403.
- 17 Liang, W.-D., T. Y. Tang, Y. J. Yang, M. T. Ko, and W.-S. Chuang, 2003. Upper-ocean
18 currents around Taiwan. *Deep Sea Research, Part II*, 50, 1085-1105.
- 19 Liu, J.T., Lin, H.-L., and Huang, J.J., 2006. A submarine canyon conduit under typhoon
20 conditions off Southern Taiwan. *Deep-Sea Research, Part I*, 53, 223-240.
- 21 Liu, J.P., C.S. Liu, K.H. Xu, J.D. Milliman, J.K. Chiu, S.J. Kao, and S.W. Li, 2008. Flux and
22 fate of small mountainous rivers derived sediments into the Taiwan Strait. *Journal of*
23 *Geology*, 256, 65-76.
- 24 Liu, C.-C., Chiu Y.-F., Lee J.-F., Su C.-H., Chen M.-T., Lee C.-T. ,Tu L.-F., and Cheng P.-C.,
25 2014. Enhancement of marine meteorology simulation technology on coastal and harbor areas
26 (1/2), Institute of Harbor & Marine Technology Center, Ministry of Transportation and
27 Communication, Taichung City, Taiwan (R.O.C.), ISBN978-986-04-0453-1, 2014.
- 28 Meiburg, E. and Kneller, B., 2010. Turbidity currents and their deposits. *Annual Review of*
29 *Fluid Mechanics*, 42, 135-156.

- 1 Mellor, G.L. and Yamada, T., 1982. Development of a turbulent closure model for
2 geophysical fluid problems. *Review of Geophysical and Space Physics*, 20, 851–875.
- 3 Milliman, J.D., and S.-J. Kao, 2005. Hyperpycnal discharge of fluvial sediment to the ocean:
4 Impact of super-typhoon Herb (1996) on Taiwanese rivers. *Journal of Geology*, 113, 503-516.
- 5 Milliman, J.D., Lin, S.W., Kao, S.J., Liu, J.P., Liu, C.S., Chiu, J.K., Lin, Y.C., 2007. Short-
6 term changes in seafloor character due to flood-derived hyperpycnal discharge: typhoon
7 Mindulle, Taiwan, July 2004. *Geology*, 35, 779–782.
- 8 Milliman, J.D., Syvitski, J.P.M., 1992. Geomorphic/tectonic control of sediment discharge to
9 the ocean: the importance of small mountainous rivers. *Journal of Geology*, 100, 525–544.
- 10 Mirabito, C., P. Haley, Jr., P.F.J. Lermusiaux, and W.G. Leslie, 2013. A river discharge
11 model for coastal Taiwan during typhoon Morakot. Cambridge: Massachusetts Institute of
12 Technology, 21 p.
- 13 Mirabito, C., P. Haley, Jr., P.F.J. Lermusiaux, and W.G. Leslie, 2012. A River Discharge
14 Model for Coastal Taiwan during Typhoon Morakot, Rep. MSEAS-13, MIT, Cambridge,
15 MA.
- 16 Nash, D.B., 1994. Effective sediment-transporting discharge from magnitude–frequency
17 analysis. *Journal of Geology*, 102, 79–95.
- 18 O'Donnell, J., 1990. The formation and fate of a river plume: a numerical model. *Journal of*
19 *Physical Oceanography* 20, 551–569.
- 20 Orton, G.J., Reading, H.G., 1993. Variability of deltaic processes in terms of sediment supply,
21 with particular emphasis on grain size. *Sedimentology*, 40, 475–512.
- 22 Osadchiev, A.A., Zavialov, P.O., 2013. Lagrangian model of a surface-advected river plume.
23 *Continental Shelf Research*, 58, 96–106.
- 24 Ross, O.N., and Sharples, J., 2004. Recipe for 1-D Lagrangian particle tracking models in
25 space-varying diffusivity. *Limnology and Oceanography: Methods*, 2, 289-302.
- 26 Rudnick, D.L., S. Jan, L. Centurioni, C.M. Lee, R.-C. Lien, J. Wang, D.-K. Lee, R.-S. Tseng,
27 Y.Y. Kim, and C.-S. Chern, 2011. Seasonal and mesoscale variability of the Kuroshio near its
28 origin. *Oceanography*, 24, 52-63.

- 1 Shen, H.-C., 2012. Topography Induced Flow Variations between Taitung-Lutao off
2 Southeast Taiwan. Kaoshiung, Taiwan: Institute of Applied Marine Physics and Undersea
3 Technology, National Sun Yat-sen University, Master's thesis, 138p.
- 4 Smagorinsky, J., 1963. General circulation experiments with the primitive equation. 1. The
5 basic experiment. *Monthly Weather Review*, 91, 99–165.
- 6 Spagnol, S., E. Wolanski, E. Deleersnijder, R. Brinkman, F. McAllister, B. Cushman-Roisin,
7 and E. Hanert, 2002. An error frequently made in the evaluation of advective transport in two-
8 dimensional Lagrangian models of advection/diffusion in coral reef waters. *Marine Ecology*
9 *Progress Series*, 235, 299-302.
- 10 Stokes, G.G., 1851. On the effect of the internal friction of fluids on the motion of pendulums.
11 *Cambridge Philosophical Transactions*, 9, 8 –106.
- 12 Su, C.-C., Tseng, J.-Y., Hsu, H.-H., Chiang, C.-S., Yu, H.-S., Lin, S., and Liu, J.T., 2012.
13 Records of submarine natural hazards off SW Taiwan. *Geological Society, London, Special*
14 *Publications*, 361, 41-60.
- 15 Syvitski, J.P.M. and Saito, Y., 2007. Morphodynamics of Deltas Under the Influence of
16 Humans. *Global Planetary Change*, 57, 261–282.
- 17 Talling, P. J., Paull, C. K., and Piper, D. J., 2013. How are subaqueous sediment density flows
18 triggered, what is their internal structure and how does it evolve? Direct observations from
19 monitoring of active flows. *Earth-Science Reviews*, 125, 244-287.
- 20 Visser, A.W., 1997. Using random walk models to simulate the vertical distribution of
21 particles in a turbulent water column. *Marine Ecology Progress Series*, 158, 275-281.
- 22 Walsh, J.P. and Nittrouer, C.A., 2009. Understanding fine-grained river-sediment dispersal on
23 continental margins. *Marine Geology*, 263, 34-45.
- 24 Warrick, J.A., 2014. Eel River margin source-to-sink sediment budgets: Revisited. *Marine*
25 *Geology*, 351, 25-37.
- 26 Warrick, J.A., Milliman, J.D., 2003. Hyperpycnal sediment discharge from semiarid southern
27 California rivers: implications for coastal sediment budgets. *Geology*, 31, 781–784.
- 28 Wright, L.D., Friedrichs, C.T., Kim, S.C., Scully, M.E., 2001. Effects of ambient currents and
29 waves on gravity-driven sediment transport on continental shelves. *Marine Geology*, 175, 25-
30 45.

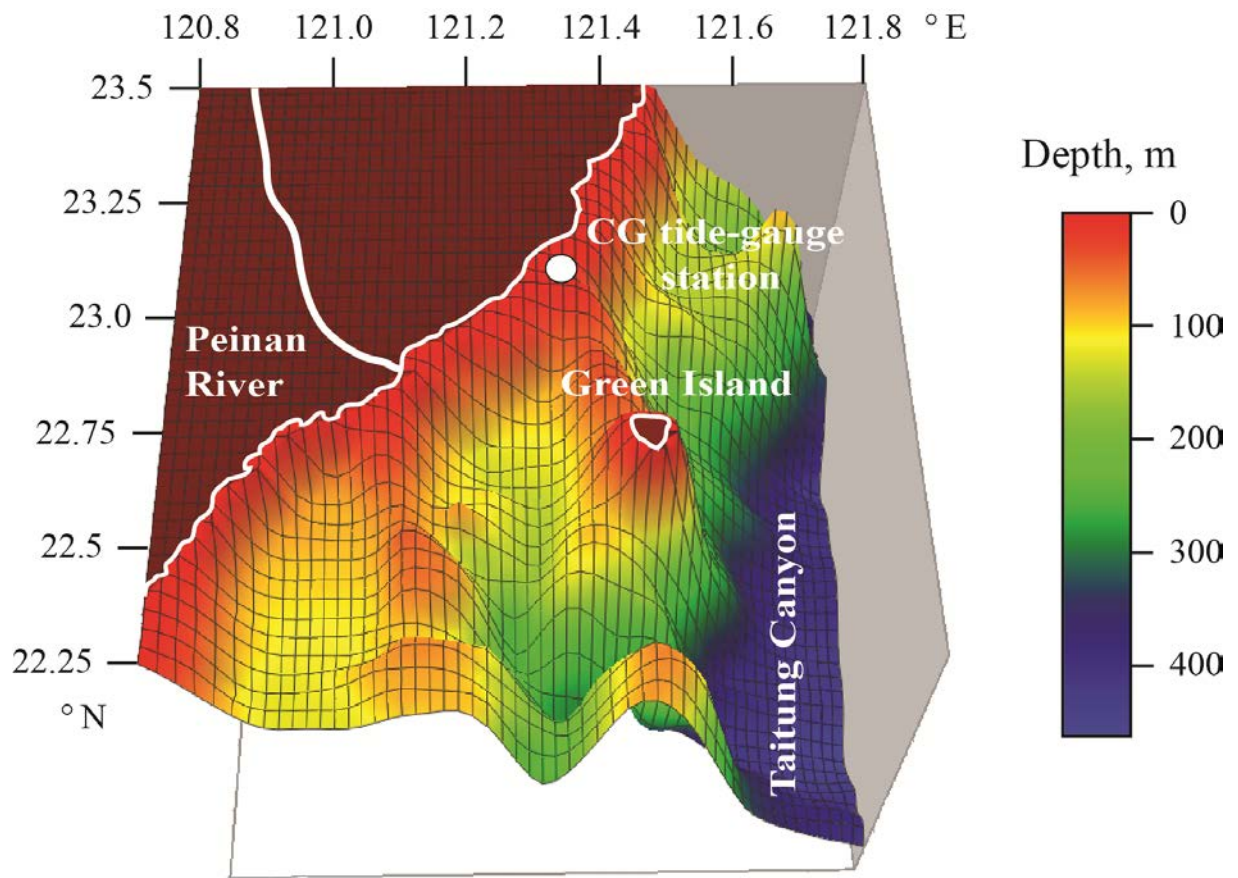
- 1 Wu, L., J. Liang, C.-C. Wu, 2011. Monsoonal influence on Typhoon Morakot (2009). Part I:
2 Observational Analysis. *Journal of Atmospheric Science*, 68, 2208-2220.
- 3 Wyrtky, K., 1961. Scientific results of marine investigations of the South China Sea and the
4 Gulf of Thailand. In *NAGA Report*, Vol. 2, The University of California, Scripps Institution
5 of Oceanography, La Jolla, USA.
- 6 Yu, H.S., 2006. Hyperpycnal discharge of fluvial sediment to the ocean: impact of
7 supertyphoon herb (1996) on Taiwanese rivers: a discussion. *Journal of Geology*, 114, 763–
8 765.
- 9 Yuan, Y., C. Liu, Z. Pan and S. Zheng, 1996. Circulation east of Taiwan and in the East
10 China Sea and east of Ryukyu Islands during early summer 1985. *Acta Oceanologica Sinica*,
11 15, 423–435.
- 12 Yuan, Y., Y. Liu, C. Liu and J. Su, 1998. The Kuroshio east of Taiwan and the currents east
13 of the Ryukyu Islands during October of 1995. *Acta Oceanologica Sinica*, 17, 1–13.
- 14 Zu, T., Gan J. and S.Y. Erofeeva, 2008. Numerical study of the tide and tidal dynamics in the
15 South China Sea. *Deep-Sea Research*, I, 55, 137–154.
- 16



the region of numerical modelling

the region of field work

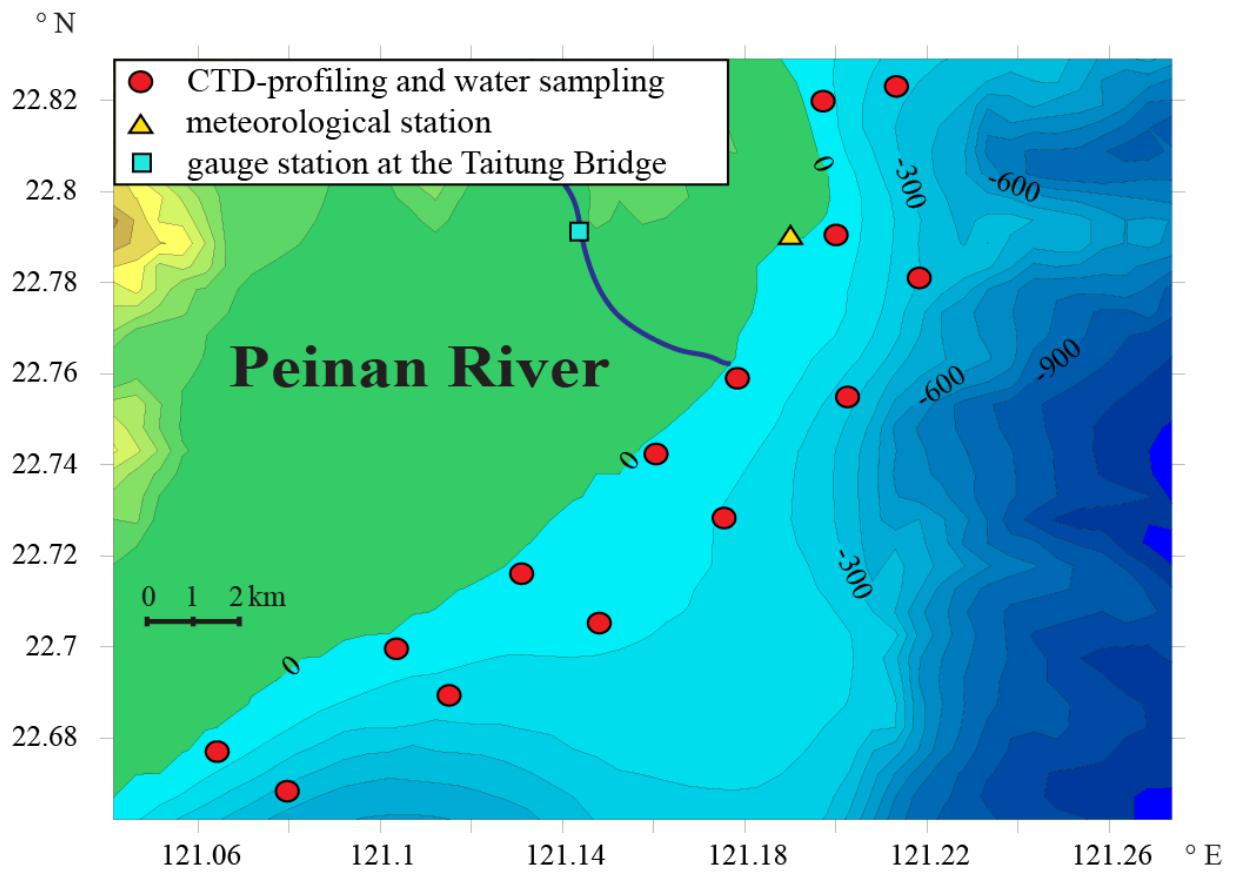
- 1
- 2 Figure 1. Bathymetry of Taiwan coastal area and deposition of the study regions at the steep
- 3 south-eastern shore adjacent to the Peinan River estuary.
- 4



1

2 Figure 2. Bathymetry of the region of numerical modelling illustrating deposition of the
 3 Green Island, Taitung Canyon, two submarine canyons east of the Green Island as well as
 4 locations of the Peinan River and the CG tide-gauge station.

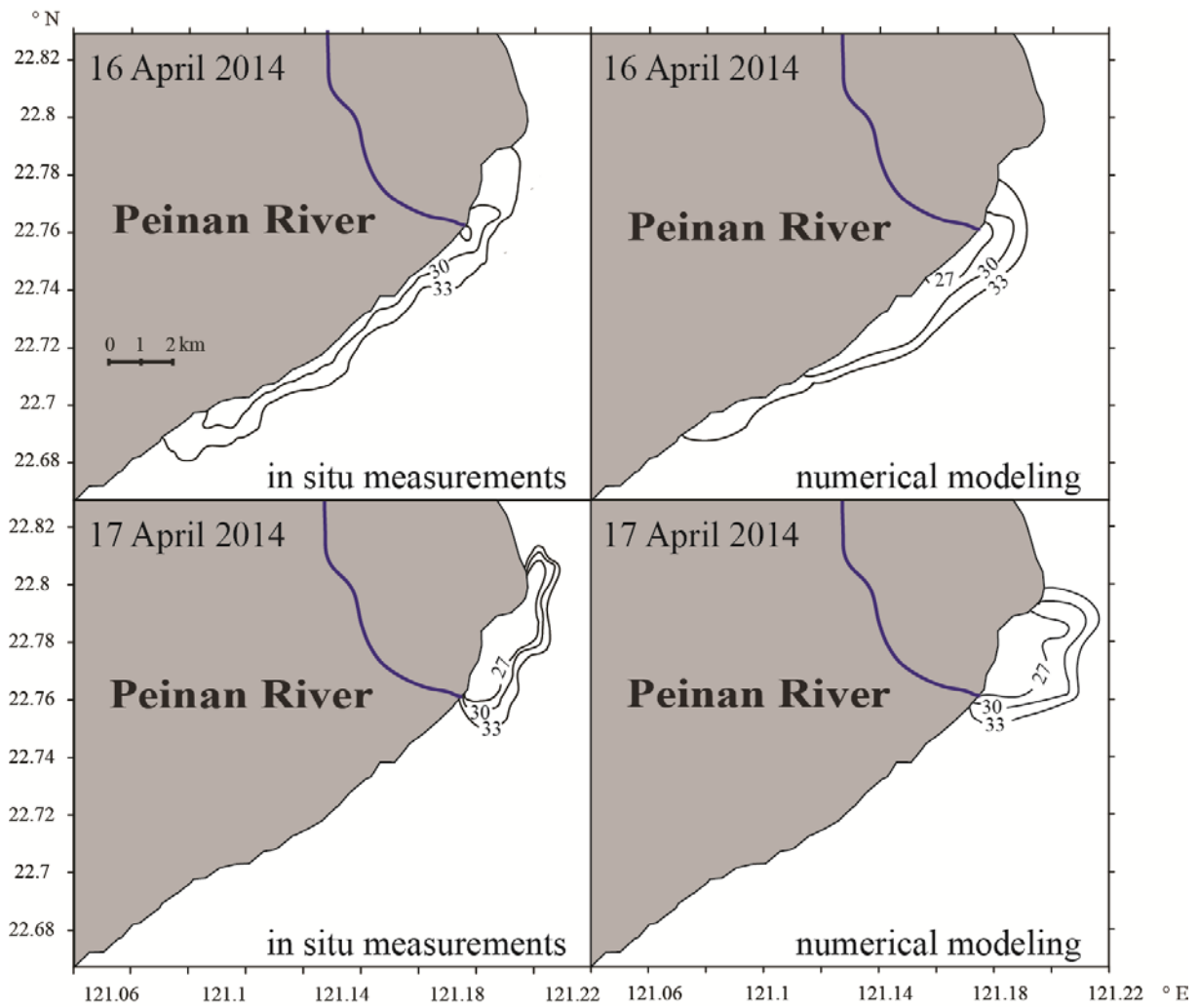
5



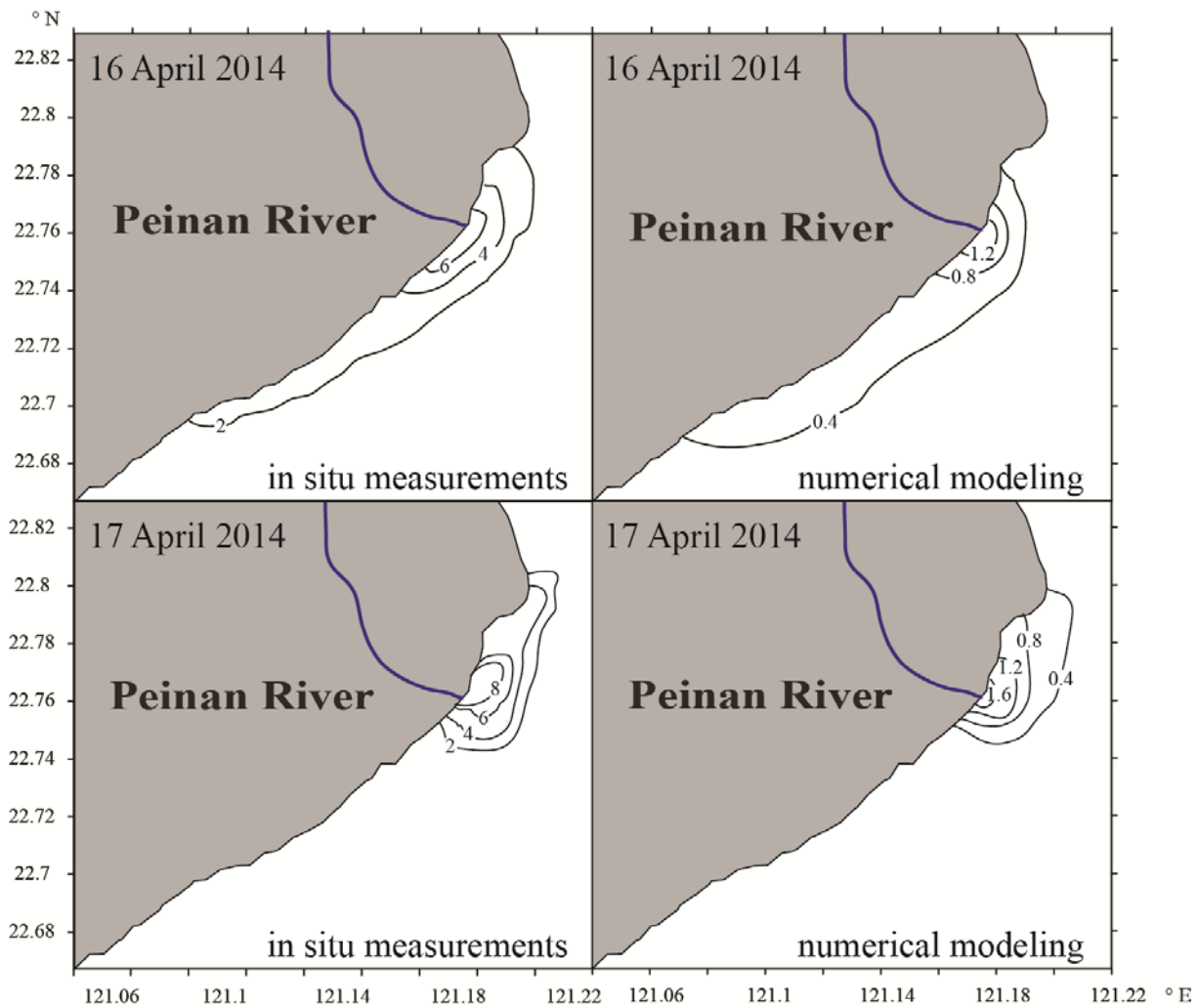
1

2 Figure 3. Bathymetry and location of stations at the region of field work conducted on 15-17
 3 April 2014.

4



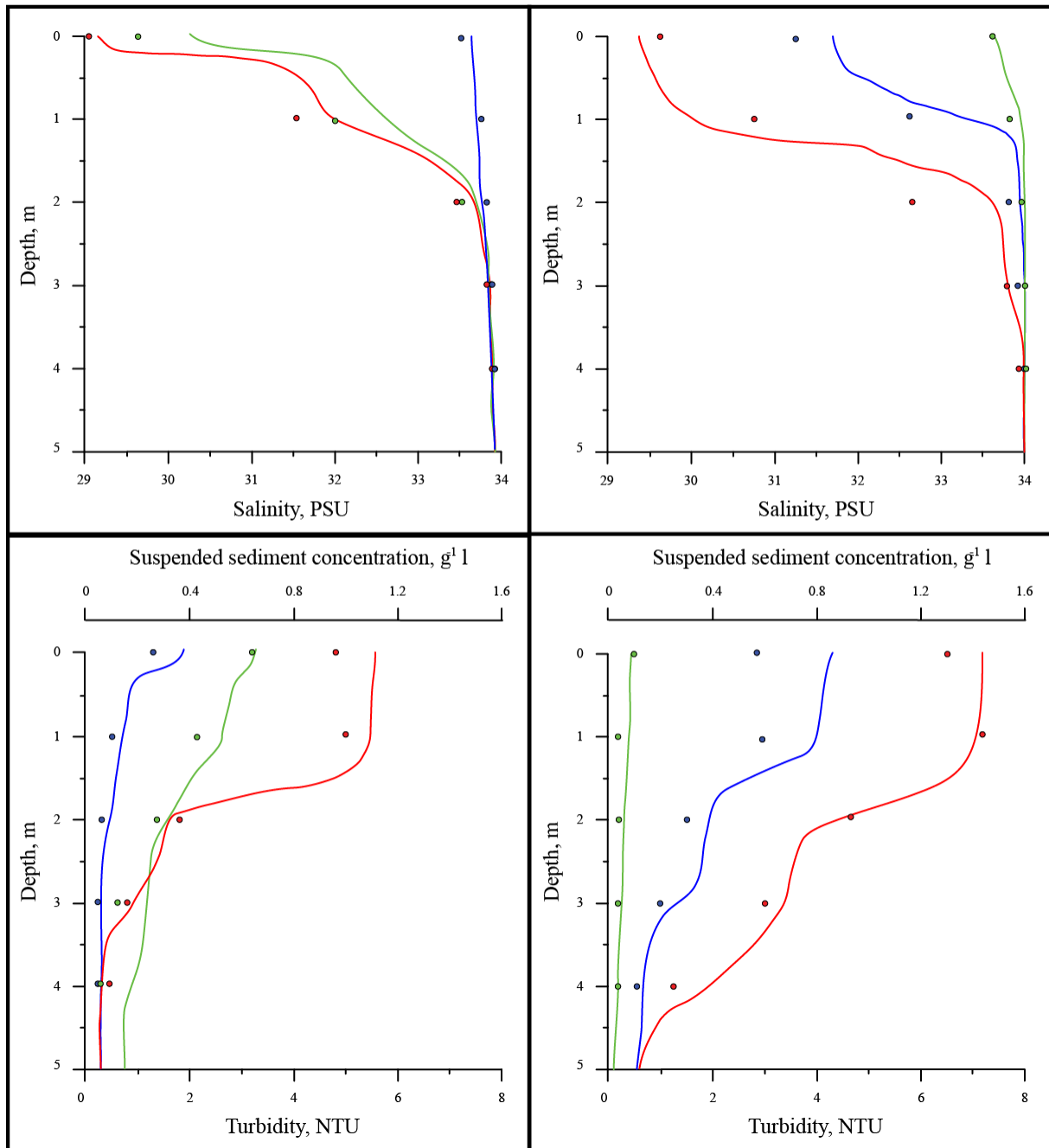
1
 2 Figure 4. Surface salinity distribution (27, 30, and 33 PSU isolines) illustrating deposition and
 3 internal structure of the Peinan river plume obtained from the in situ measurements (left
 4 panels) and simulated by the numerical model (right panels) on 16 April 2014 (top panels)
 5 and 17 April 2014 (bottom panels).
 6



1
 2 Figure 5. Surface distribution of turbidity obtained from the in situ measurements (left panels;
 3 2, 4, 6, and 8 NTU isolines) and suspended sediment concentration simulated by the
 4 numerical model (right panels; 0.4, 0.8, 1.2, and 1.6 g l⁻¹ isolines) on 16 April 2014 (top
 5 panels) and 17 April 2014 (bottom panels).
 6

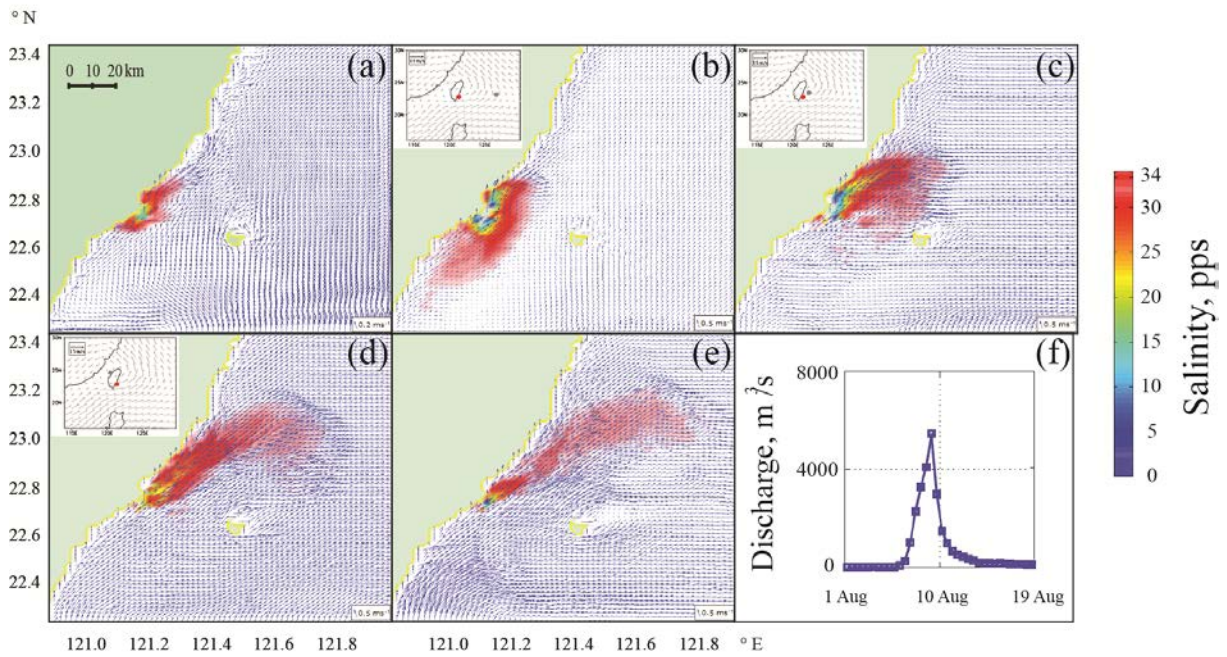
16 April 2014

17 April 2014

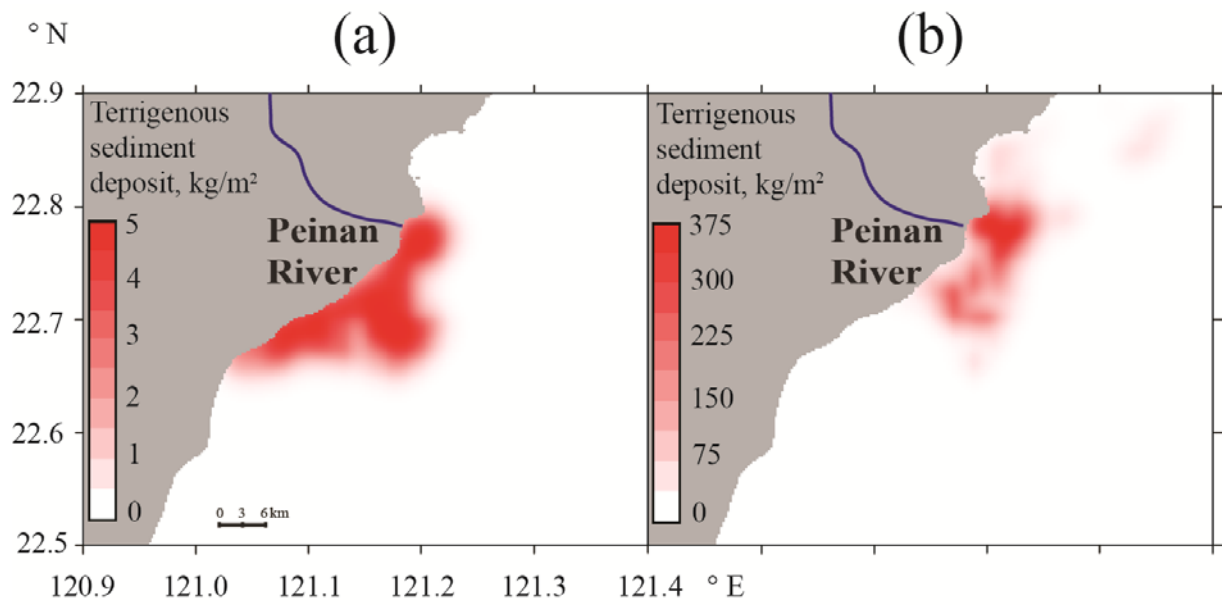


1
 2 Figure 6. Vertical profiles of salinity (top panels) and turbidity (bottom panels) obtained from
 3 the in situ measurements (solid lines) at stations 8 (green), 10 (red), and 12 (blue) on 16 April
 4 2014 (left panels) and 17 April 2014 (right panels) and the related values of salinity (top
 5 panels) and suspended sediment concentrations (bottom panels) simulated by the numerical
 6 model (circles). Value of 1 NTU of the in situ turbidity measurements was assumed to
 7 correspond to value of 0.2 g l^{-1} of the simulated suspended sediment concentration.

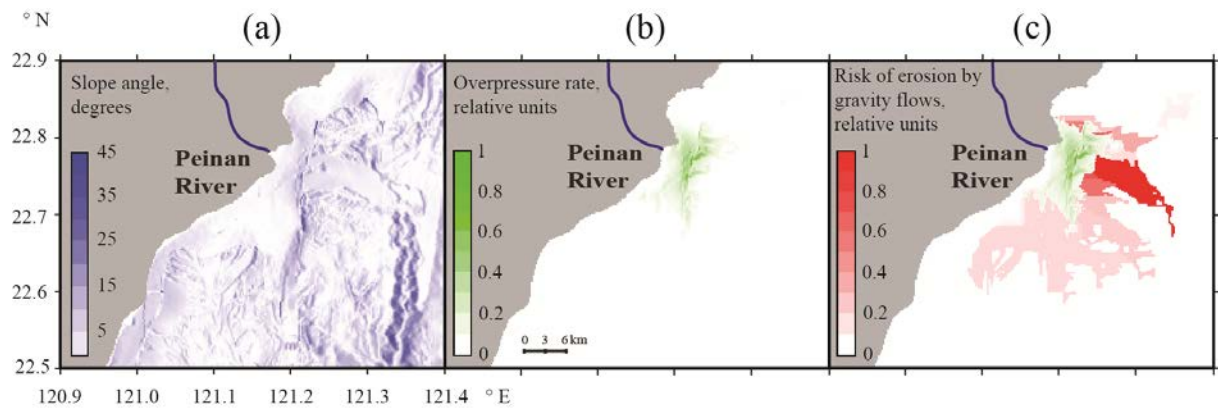
8



1
 2 Figure 7. The Peinan River plume under typhoon conditions before (a), on the first (b), the
 3 second (c), the third (d), and the fifth (e) day of typhoon simulation. The left bottom panel (f)
 4 shows the discharge rate of the Peinan River in August 2009 during the typhoon Morakot
 5 (after Mirabito et al., 2012). Deposition of the center of 700-hPa typhoon (grey solid dot) and
 6 the Peinan River estuary (red solid star) are shown in the insets in (b)-(d) (after Wu et al.,
 7 2011).
 8



1
 2 Figure 8. Simulated distribution of fine sediments deposited to the seabed at the study area
 3 under moderate (a) and flooding (b) forcing conditions.
 4



1
 2 Figure 9. Bottom topography gradient at the region of numerical modelling (a), distribution of
 3 the overpressure rate (b) after typhoon conditions and potential paths of the related gravity
 4 flows (c).